

High-resolution differential phase contrast imaging using a magnifying projection geometry with a microfocus x-ray source

Martin Engelhardt^{a)}

Siemens AG, Corporate Technology, 81739 Munich, Germany and Physik Department, Technische Universität München, 85747 Garching, Germany

Joachim Baumann and Manfred Schuster

Siemens AG, Corporate Technology, 81739 Munich, Germany

Christian Kottler, Franz Pfeiffer, Oliver Bunk, and Christian David

Paul Scherrer Institut, 5232 Villigen PSI, Switzerland

(Received 30 March 2007; accepted 6 May 2007; published online 30 May 2007)

Differential x-ray phase contrast imaging using a grating interferometer was combined with a magnifying cone beam geometry using a conventional microfocus x-ray tube. This brings the advantages of a magnifying cone beam setup, namely, a high spatial resolution in the micron range and the possibility of using an efficient, low resolution detector, into differential phase contrast imaging. The authors present methodical investigations which show how the primary measurement signal depends on the magnification factor. As an illustration of the potential of this quantitative imaging technique, a high-resolution x-ray phase contrast tomography of an insect is presented.

© 2007 American Institute of Physics. [DOI: 10.1063/1.2743928]

X-ray absorption imaging is a common tool for medical diagnostics and industrial nondestructive testing. However, if weakly absorbing samples are under investigation, the applicability of conventional absorption x-ray imaging is limited. In this case, phase sensitive x-ray imaging, which uses the phase shift rather than the absorption as an imaging signal, can overcome these shortcomings, since it offers a significantly increased contrast.¹ Various x-ray phase contrast techniques exist,²⁻⁶ but only propagation based methods³ and recently developed grating based methods⁴⁻⁶ work well with a broad energy spectrum and therefore they can be combined with laboratory x-ray sources. With grating based methods, the differential phase contrast (first derivative of the phase shift) is measured. This is an advantage in comparison to propagation based methods, as these produce data containing the second derivative of the phase shift. For propagation based methods, a detector with high spatial resolution is imperative. Using previous grating based methods the spatial resolution is limited by the detector, which also necessitates a high detector resolution in many cases. In this letter, we present a setup for differential phase contrast imaging in combination with a microfocus x-ray source and projection magnification. This makes detector systems with moderate spatial resolution applicable for high-resolution phase contrast imaging. Thus, thick scintillators with good detection efficiency even at higher energies can be used.

An outline of the setup is shown in Fig. 1. The phase grating g_1 , with lines showing negligible x-ray attenuation, but a phase shift of π , acts as a beam splitter. It divides the incoming beam essentially into the +1st and -1st diffraction orders. Downstream of g_1 , the diffracted beams interfere and form a periodic interference pattern in planes parallel to g_1 . Due to the fractional Talbot effect,⁷ this pattern exhibits a maximum modulation at distances

$$d_m = m \frac{p_1^2}{8\lambda}, \quad (1)$$

for a parallel beam setup,⁶ where λ is the wavelength, p_1 the period of g_1 , and m an odd integer which corresponds to the order of the fractional Talbot distance. For a cone beam setup, these distances rescale to⁸

$$d_m^* = \frac{l}{l - d_m} d_m. \quad (2)$$

The interference pattern shows a lateral period of $p_2 = p_1/2$ for a parallel beam setup and

$$p_2^* = \frac{l}{l - d_m} \frac{p_1}{2}, \quad (3)$$

for a cone beam setup.⁶ If an extended x-ray source is used, the source size ξ must be chosen small enough so that the transversal coherence length $\Lambda_c = \lambda \times l / \xi$ at the plane of g_2 is larger than the separation $h_m = mp_1/4$ of the interfering beams, because only in this case does the interference pattern have a reasonable degree of modulation. Modifications of the incident wave front due to an object in the beam path lead to a change of the first order diffraction angle of⁵

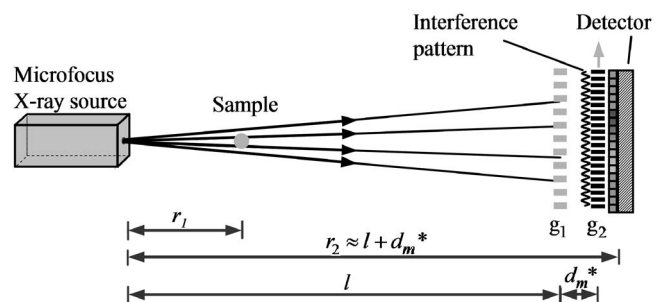


FIG. 1. Setup for differential phase contrast imaging using a projection magnification.

^{a)}Electronic mail: martin.engelhardt.ext@siemens.com

$$\Delta\alpha_{\text{PG}} = \frac{\lambda}{2\pi} \frac{\partial\phi_{\text{PG}}}{\partial x_{\text{PG}}}, \quad (4)$$

where $\partial\phi_{\text{PG}}/\partial x_{\text{PG}}$ is the differential phase shift at the phase grating plane. Thereby, the position of the interference fringes is shifted by $s = \Delta\alpha_{\text{PG}} \times d_m^*$. Consequently, a measurement of the position change of the interference fringes yields the differential phase shift caused by the object with⁶

$$\varphi = \frac{\lambda d_m}{p_2} \frac{\partial\phi_{\text{PG}}}{\partial x_{\text{PG}}}, \quad (5)$$

where $\varphi = 2\pi \times s/p_2^*$ is the lateral shift of the interference pattern. In order to determine the location of the fringes of the interference pattern, it is scanned with the absorption grating g_2 , which consists of highly absorbing bars and has a period which matches p_2^* . Thereby, a series of images is recorded at different relative positions of the two gratings.⁶ The method also works with a polychromatic energy spectrum, because the interference fringes have a high modulation⁶ for a relatively large energy interval. A simple approach to account for a polychromatic energy spectrum is to assign an effective mean energy, derived from transmission data, to the measurement.⁵

Our setup for grating based differential phase contrast imaging with a magnifying cone beam geometry comprised a Hamamatsu microfocus tube with a W target and a focal spot size ξ of approximately $8 \mu\text{m}$ (manufacturer's instructions based on DIN EN 12543-5), operated at 50 kV and $100 \mu\text{A}$. A source-detector distance of $r_2 = 1770 \text{ mm}$ was chosen. The setup was optimized for a photon energy of 17.5 keV which results in a structure height of $23 \mu\text{m}$ for the silicon phase grating, yielding a phase shift of π . Two different phase gratings were available with periods p_1 of 3.94 and $3.82 \mu\text{m}$, for application with an intergrating distance set to the first ($m = 1$) and the third ($m = 3$) fractional Talbot distance (calculated for 17.5 keV photon energy), respectively. They yield a lateral period of the interference pattern of $2 \mu\text{m}$ for $m = 1$ and $m = 3$. This corresponds to the period of the absorption grating g_2 , which consisted of $12 \mu\text{m}$ thick gold absorber structures. A charge coupled device camera coupled to a $600 \mu\text{m}$ thick Hamamatsu CsI scintillator using an objective lens was applied as a detector system, yielding an effective pixel size of $100 \mu\text{m}$.

In order to study the physical effects in grating based differential phase contrast imaging, a cylindrical polymethyl methacrylate (PMMA) rod with a diameter of 2.1 mm was investigated as a test object. For this measurement, the distance between g_1 and g_2 was set to the first fractional Talbot distance ($m = 1$). Different magnifications $M = r_2/r_1$ between 2 and 14 were selected by varying r_1 . The axis of the rod was parallel to the grating lines. The values of the fringe shift φ and thus the differential phase shift $\partial\phi_{\text{PG}}/\partial x_{\text{PG}}$ recorded for the cylinders along a straight line perpendicular to the axis are presented in Fig. 2(a). As apparent from the figure, these values vary with M and r_1 , respectively. The total x-ray phase shift caused by the object is denoted by $\phi_{\text{obj}}(x_{\text{obj}})$ at the position of the object and $\phi_{\text{PG}}(x_{\text{PG}})$ at the position of the phase grating. These two functions are related to each other by $\phi_{\text{obj}}(x_{\text{obj}}) = \phi_{\text{PG}}(x_{\text{PG}})$, with $x_{\text{obj}} = x_{\text{PG}} \times r_1/l$. Therefore, the differential phase shift follows the basic relationship

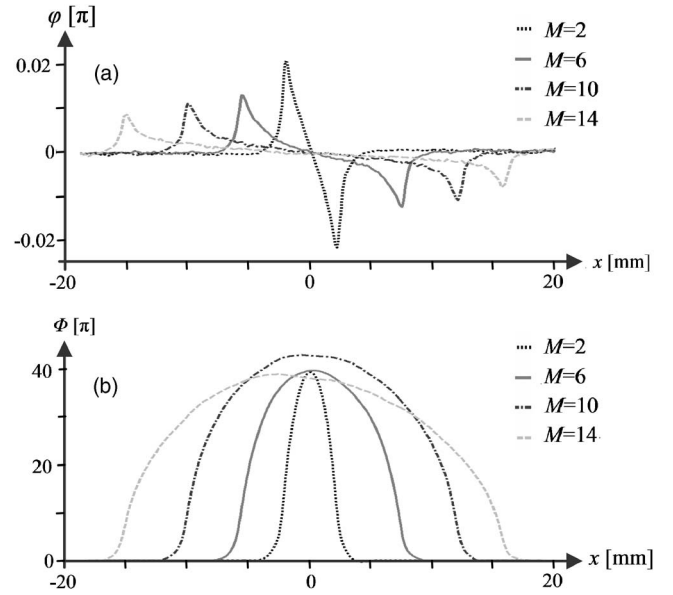


FIG. 2. Shift of the interference fringes (a) and the total phase shift derived (b) for a cylindrical PMMA rod with a diameter of 2.1 mm using different magnifications. The intergrating distance was set to the first fractional Talbot distance.

$$\frac{\partial\phi_{\text{PG}}}{\partial x_{\text{PG}}} = \frac{r_1}{l} \frac{\partial\phi_{\text{obj}}}{\partial x_{\text{obj}}}. \quad (6)$$

This gives a mathematical proof for the decay of $\partial\phi_{\text{PG}}/\partial x_{\text{PG}}$ with decreasing r_1 . The situation is visualized in Fig. 3. The differential phase shift due to the object causes a refraction of the incident beam of

$$\Delta\alpha_{\text{obj}} = \frac{\lambda}{2\pi} \frac{\partial\phi_{\text{obj}}}{\partial x_{\text{obj}}}, \quad (7)$$

independent of the projection magnification. Due to the large distance between the object and the phase grating, the refracted beam hits g_1 at a different position. The angular deviation $\Delta\alpha_{\text{PG}}$ between the refracted and the undisturbed (dashed) beam depends on r_1 and is smaller than $\Delta\alpha_{\text{obj}}$, cf. Fig. 3. From geometry, it follows that

$$\Delta\alpha_{\text{PG}} = \frac{r_1}{l} \Delta\alpha_{\text{obj}}. \quad (8)$$

In combination with Eqs. (4) and (7), this gives a graphic explanation of Eq. (6). For the setup applied, the PMMA cylinders show an x-ray transmission of 91.5%. By comparison with tabulated values,⁹ an effective mean photon energy of 23.6 keV is deduced. From the differential phase shift derived using Eq. (5) with this effective energy, the total phase shift was calculated [Fig. 2(b)]. The values obtained at

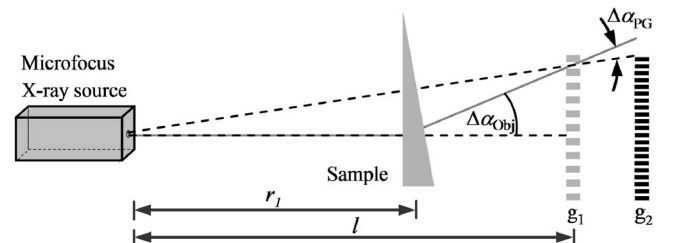


FIG. 3. Determination of a correlation between $\Delta\alpha_{\text{PG}}$ and $\Delta\alpha_{\text{obj}}$.

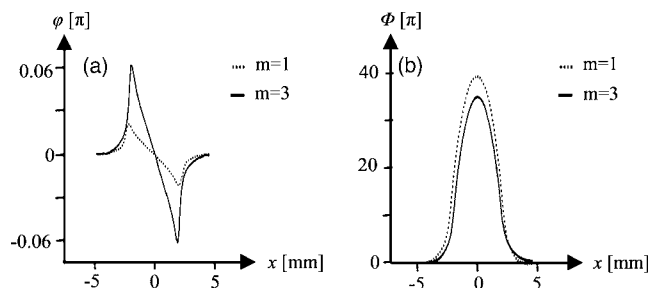


FIG. 4. Shift of the interference fringes (a) and the total phase shift derived (b) for a cylindrical PMMA rod with a diameter of 2.1 mm using a magnification of $M=2$. The intergrating distance was set to the first ($m=1$) and third ($m=3$) fractional Talbot distance.

the center of the rods are all in agreement with the calculated value of 38π (Ref. 9).

These measurements prove that the lateral shift of the interference fringes φ decreases with the object magnification, which makes the measurement less sensitive. This can be compensated by enlarging the distance between the phase and the analyzer grating. The measurement described above was repeated for a magnification of $M=2$ with an intergrating distance set to the third fractional Talbot distance ($m=3$). The results are presented in Fig. 4. For $m=3$, the primary measurement signal φ is three times larger in comparison to that for $m=1$ [Fig. 4(a)], whereas the total phase shift is identical [Fig. 4(b)]. This is in agreement with Eq. (5).

These studies clearly show that the experiment allows us to determine quantitatively the total phase shift. Therefore, the data can be used for a tomographic reconstruction of the refractive index decrement δ . In order to demonstrate the capabilities of the method, a phase tomography of a wasp was acquired with the setup described above, using 360 projections with a total exposure time of approximately 33 h and a magnification factor M of 3.5. A rendered visualization of the refractive index decrement δ distribution is presented in Fig. 5. The result clearly shows that details smaller than a detector pixel of $100\ \mu\text{m}$ can be resolved.

Summing up, a setup for high-resolution differential phase contrast imaging using a magnifying cone beam geometry was presented. It was shown, both theoretically and experimentally, that the primary measurement signal and the differential phase shift determined are lowered as the magnification is increased. This turned out to be imperative in order to determine the total phase shift correctly. A simple possibility for compensating this effect by an increase of the primary measurement signal was demonstrated. Finally, the capabilities of the method were demonstrated by a phase tomography of an insect.

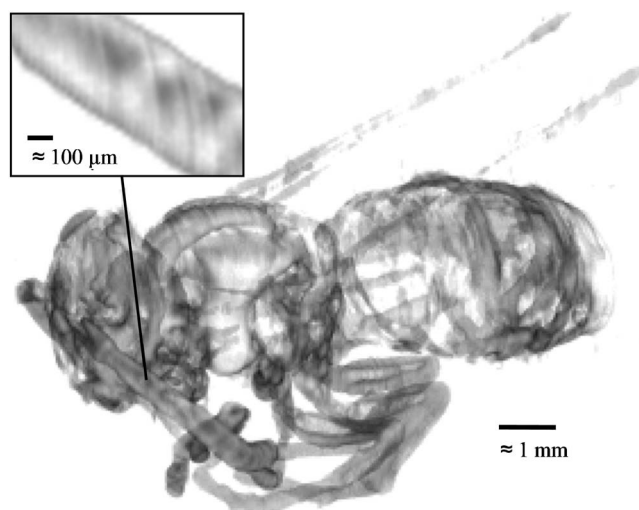


FIG. 5. Phase tomography of a wasp. The image shows a quantitative representation of the refractive index decrement δ .

The authors would like to thank Peter Böni and Burkhard Schillinger of Technische Universität München for fruitful discussions.

- ¹R. Fitzgerald, *Phys. Today* **53**(7), 23 (2000); A. Momose, *Opt. Express* **11**, 2303 (2003); A. Momose, *Jpn. J. Appl. Phys., Part 1* **44**, 6355 (2005).
- ²U. Bonse and M. Hart, *Appl. Phys. Lett.* **6**, 155 (1965); A. Momose, T. Takeda, Y. Itai, and K. Hirano, *Nat. Med.* **2**, 473 (1996); V. N. Ingal and E. A. Beliaevskaya, *J. Phys. D* **28**, 2314 (1995); T. J. Davis, D. Gao, T. E. Grueyev, A. W. Stevenson, and A. W. Wilkins, *Nature (London)* **373**, 595 (1995); L. D. Chapman, W. C. Thomlinson, R. E. Johnson, D. Washburn, E. Pisano, N. Gmuer, Z. Zhong, R. Menk, F. Arfelli, and D. Sayers, *Phys. Med. Biol.* **42**, 2015 (1997).
- ³A. Snigirev, I. Snigireva, V. Kohn, S. Kuznetsov, and I. Schelkov, *Rev. Sci. Instrum.* **66**, 5486 (1995); S. W. Wilkins, T. E. Gureyev, D. Gao, A. Pogany, and A. W. Stevenson, *Nature (London)* **384**, 335 (1996); P. Cloetens, W. Ludwig, J. Baruchel, D. van Dyck, J. van Landuyt, J. P. Guigay, and M. Schlenker, *Appl. Phys. Lett.* **75**, 2912 (1999); K. A. Nugent, T. E. Gureyev, D. F. Cookson, D. Paganin, and Z. Barnea, *Phys. Rev. Lett.* **77**, 2961 (1996); S. C. Mayo, T. J. Davis, T. E. Gureyev, P. R. Miller, D. Paganin, A. Pogany, A. W. Stevenson, and S. W. Wilkins, *Opt. Express* **11**, 2289 (2003); A. G. Peele, F. De Carlo, P. J. McMahon, B. B. Dhal, and K. A. Nugent, *Rev. Sci. Instrum.* **76**, 083707 (2005).
- ⁴C. David, B. Nöhammer, and H. H. Solak, *Appl. Phys. Lett.* **81**, 3287 (2002); T. Weitkamp, B. Nöhammer, A. Diaz, and C. David, *ibid.* **86**, 054101 (2005).
- ⁵F. Pfeiffer, T. Weitkamp, O. Bunk, and C. David, *Nat. Phys.* **2**, 258 (2006).
- ⁶T. Weitkamp, A. Diaz, C. David, F. Pfeiffer, M. Stampanoni, P. Cloetens, and E. Ziegler, *Opt. Express* **13**, 6296 (2005).
- ⁷J. P. Guigay, S. Zabler, P. Cloetens, C. David, R. Mokso, and M. Schlenker, *J. Synchrotron Radiat.* **11**, 476 (2004); F. Pfeiffer, O. Bunk, C. Schulze, A. Diaz, T. Weitkamp, C. David, J. F. van der Veen, I. Vartanyants, and I. K. Robinson, *Phys. Rev. Lett.* **94**, 163104 (2005).
- ⁸*Diffraction Physics*, 3rd revised ed., edited by J. M. Cowley (Elsevier, Amsterdam, 1995), p. 21.
- ⁹B. L. Henke, E. M. Gullikson, and J. C. Davis, *At. Data Nucl. Data Tables* **54**, 181 (1993).